


Injured Cardiac Tissue-Targeted Delivery of TGFβ1 siRNA by FAP Aptamer-Functionalized Extracellular Vesicles Promotes Cardiac Repair

Ji-Young Kang¹, Dasom Mun¹, Malgeum Park¹, Gyeongseo Yoo², Hyoeun Kim³, Nuri Yun⁴, Boyoung Joung^{1,2} 

¹Division of Cardiology, Yonsei University College of Medicine, Seoul, 03722, Republic of Korea; ²Graduate School of Medical Science, Brain Korea 21 Project, Yonsei University College of Medicine, Seoul, 03722, Republic of Korea; ³Department of Biochemistry and Molecular Biology, Yonsei University College of Medicine, Seoul, 03722, Republic of Korea; ⁴GNTPharma Science and Technology Center for Health, Incheon, 21983, Republic of Korea

Correspondence: Boyoung Joung, Division of Cardiology, Yonsei University College of Medicine, Seoul, 03722, Republic of Korea, Tel +82-2-2228-8447, Fax +82-2-2227-7732, Email cby6908@yuhs.ac; Nuri Yun, GNTPharma Science and Technology Center for Health, Incheon, 21983, Republic of Korea, Tel +82-31-8005-9910, Fax +82-31-8005-9917, Email yunnuri@hanmail.net

Purpose: Small-interfering RNA (siRNA) therapy holds significant potential for treating cardiac injury; however, its clinical application is constrained by poor blood stability and insufficient cellular uptake. Extracellular vesicles (EVs) have emerged as an effective delivery system for siRNA in vivo; but their lack of specific cell or tissue-targeting ability remains a major challenge. Thus, we aimed to develop an EV-based delivery system capable of targeted delivery of therapeutic siRNA to injured cardiac tissue for cardiac repair.

Methods: To identify fibroblast activation protein (FAP) as a potential target for delivery to injured cardiac tissue, we analyzed cardiac tissues from patients with heart failure and angiotensin II (Ang II)-treated mice. Injured cardiac tissue-targeting EVs were developed by embedding a cholesterol-conjugated FAP aptamer, which specifically targets FAP, onto human serum-derived EVs (hEV).

Results: Our findings revealed that FAP is upregulated after cardiac injury, highlighting its potential as a target for siRNA delivery to injured cardiac tissues. We successfully developed FAP aptamer-functionalized hEV (hEV@FAP) and confirmed their typical EV characteristics, including morphology, size distribution, zeta potential, and marker protein expression. In addition, hEV@FAP demonstrated high targeting selectivity to FAP-positive regions both in vitro and in vivo. To treat cardiac injury, hEV@FAP were loaded with TGFβ1 siRNA (siTGFβ1), identified as a molecular target for cardiac repair. In Ang II-treated mice, intravenous administration of hEV@FAP-siTGFβ1 effectively reduced Ang II-induced TGFβ1 expression in cardiac tissues, attributed to the protective and targeting capabilities of hEV@FAP. Consequently, hEV@FAP-siTGFβ1 significantly improved cardiac function, reduced myocardial fibrosis, and decreased cardiomyocyte cross-sectional area ($P < 0.05$) without inducing systemic toxicity.

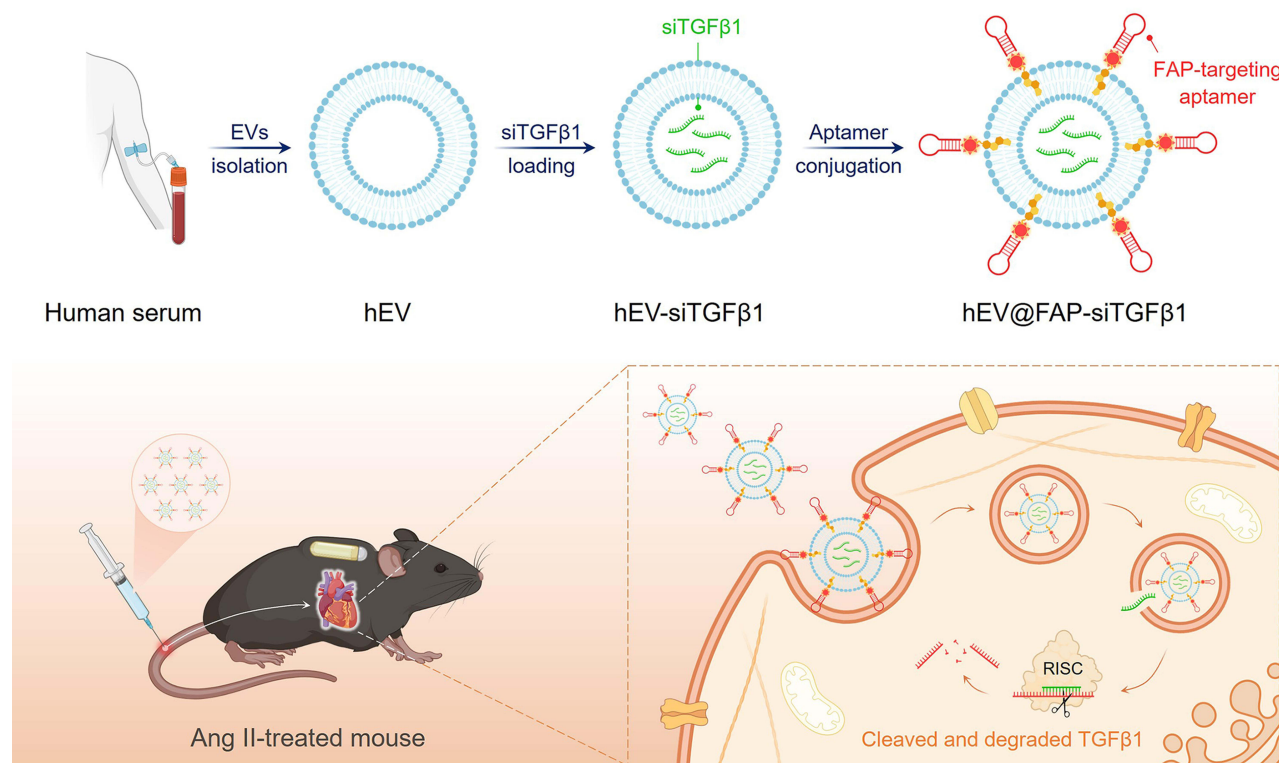
Conclusion: hEV@FAP represents a novel approach for targeted delivery of therapeutic siRNA to injured cardiac tissues, providing a promising nanomedicine for cardiac repair.

Keywords: cardiac injury, fibroblast activation protein, extracellular vesicles, small-interfering RNA, transforming growth factor beta 1

Introduction

Cardiac injury is a leading cause of morbidity and mortality worldwide, with detrimental effects including cell death, inflammation, fibrosis, and hypertrophy, ultimately resulting in irreversible cardiac structural remodeling and cardiac dysfunction.¹⁻⁵ Despite advancements in surgical procedures and pharmacological treatments, current therapeutic approaches primarily aim to alleviate symptoms, reduce fluid retention, and enhance cardiac contractility.^{2,3,6,7} Therefore, it is necessary to develop effective treatments that contribute to cardiac tissue repair and regeneration.

Graphical Abstract



Small-interfering RNA (siRNA), which enables specific post-transcriptional gene silencing, has garnered substantial attention as a promising therapeutic strategy for cardiac injury.^{8–12} However, its clinical application is hindered by multiple extracellular and intracellular delivery barriers, such as membrane impermeability, entrapment by the mononuclear phagocyte system (MPS), enzymatic degradation, challenges with endosomal escape, and off-target effects.^{13–15} To address these challenges, various delivery vehicles have been explored over the past few decades, including lipid- or polymer-based nanoparticles, gold nanoparticles, and mesoporous silica nanoparticles.^{15–20} Despite their potential, these nanoparticles face several limitations, such as high toxicity and immunogenicity, low biocompatibility, and poor delivery efficiency.^{15,21}

Extracellular vesicles (EVs) are nanosized, lipid bilayer-delimited particles secreted by all cell types into extracellular fluids, including peripheral blood (serum/plasma), urine, and saliva.^{22,23} EVs play vital roles in intercellular communication by transporting bioactive molecules such as nucleic acids, proteins, and lipids.²⁴ Recently, EVs have gained recognition as an ideal noninvasive diagnostic tool for various diseases, as their molecular content reflects the type and physiological state of their parental cells.^{25,26} In addition to their diagnostic potential, EVs carry bioactive molecules derived from diverse biological sources, mediating crucial pathophysiological processes such as angiogenesis, inflammation, cell survival, migration, and differentiation, making them as a promising therapeutic option for a wide range of medical conditions.^{25,27} Notably, EVs derived from multipotent stem cells (eg mesenchymal stem cells and hematopoietic stem cells) exhibit superior properties for tissue repair and regeneration; thus, they have been investigated in the field of regenerative medicine.^{25,28–30}

Beyond their applications as biomarkers and therapeutic targets, EVs are currently regarded as promising nanocarriers for siRNA delivery.^{31,32} Compared to conventional delivery systems, EVs offer several advantageous features, including minimal toxicity, low immunogenicity, high stability in circulation, and an intrinsic ability to cross biological barriers.^{33–35}

Recent studies have demonstrated that encapsulating of siRNA within EVs enhances their delivery efficiency, thereby improving therapeutic efficacy in treating various diseases.^{36–39} Despite these benefits, a significant challenge in EV-based delivery systems is that, after systemic administration, EVs predominantly accumulate in non-specific tissues such as the liver, spleen, or lung, leading to inadequate delivery to intended target cells or tissues.^{40,41} Therefore, it is crucial to develop strategies to engineer EVs capable of selectively accumulating in target cells or tissues during systemic delivery.

Recent studies have demonstrated that the targeting ability of EVs can be improved through surface modification with specific cell- or tissue-targeting moieties.^{42–44} One commonly used approach involves genetic modification, where parent cells are engineered to secrete functionalized EVs.^{45,46} However, these processes are complex, time-intensive, and less suitable for difficult-to-transfect cell types, such as primary cells and stem cells.^{46,47} In contrast, chemical modification offers a simpler and faster alternative for functionalizing EV surfaces with a diverse range of natural and synthetic ligands, including aptamers, antibodies, carbohydrates, peptides, and small molecules; thus, this approach is increasingly recognized as an efficient strategy.^{48,49} Notably, aptamers—single-stranded DNA/RNA oligonucleotides or peptides that bind to target molecules with high affinity and specificity^{50,51}—have been used to functionalize EVs for drug delivery in various diseases, particularly cancers.^{52–54} For instance, Luo et al⁵⁰ developed aptamer-conjugated EVs targeting bone marrow mesenchymal stem cells for the treatment of osteoporosis and fractures. In addition, Han et al⁵¹ generated prostate cancer cell-targeting EVs by conjugating E3 aptamers, demonstrating their potential in prostate cancer therapy.

Herein, we propose a novel strategy to mitigate cardiac injury using EVs functionalized with fibroblast activation protein (FAP)-targeting aptamer for the delivery of therapeutic siRNA. FAP, a prolyl-specific serine protease critically involved in the pathophysiological processes of cardiac remodeling, is significantly upregulated in the cardiac tissues of patients with cardiac injury compared to healthy individuals.^{55,56} Consequently, FAP has garnered increasing attention as a potential target for delivering therapeutics to injured cardiac tissues. However, no studies to date have explored the development of FAP aptamer-functionalized EVs for the treatment of cardiac injury. Therefore, this study provides proof-of-concept for an EV-based therapeutic strategy, enabling the efficient and targeted delivery of siRNA to injured cardiac tissues, thereby offering a promising approach for cardiac repair.

Materials and Methods

Cell Culture and Transfection

HEK293 cells (Korean Cell Line Bank, Seoul, Korea) were cultured in Dulbecco's modified Eagle's medium (DMEM; LM001-05, Welgene, Gyeongsan, Korea) supplemented with 10% fetal bovine serum (FBS; US-FBS-500, Young In Frontier, Seoul, Korea) and 1% penicillin-streptomycin (10378016, Gibco, Grand Island, NY, USA). Cells were maintained at 37 °C in a humidified incubator (Thermo Fisher Scientific, Waltham, MA, USA) with 5% CO₂.

When HEK293 cells reached 60–80% confluency, they were transfected with either a GFP-tagged control vector (NC; CV027, Sino Biological, Beijing, China) or GFP-tagged FAP expression vector (HG10464-ACG, Sino Biological) using Lipofectamine™ 3000 Transfection Reagent (L3000001, Thermo Fisher Scientific) according to the manufacturer's instructions. Successful transfection was confirmed by evaluating GFP signals under an inverted fluorescence microscope (Olympus, Tokyo, Japan).

Preparation of hEV@FAP-siTGFβ1

EVs were isolated from human serum using differential ultracentrifugation. Briefly, human serum was centrifuged at 300 × *g* for 10 min, 2,000 × *g* for 10 min, and 10,000 × *g* for 30 min, followed by ultracentrifugation at 100,000 × *g* for 1 h. The pelleted EVs were resuspended in phosphate-buffered saline (PBS) and ultracentrifuged again at 100,000 × *g* for 1 h. The final pellet was resuspended in PBS for subsequent experiments. Human serum was obtained from patients without progressive or serious cardiovascular disease attending Yonsei University (Seoul, Korea) Health System after providing informed consent. Clinical profiles of the patients are presented in [Table S1](#). This study was approved by the local ethics committee (Institutional Review Board of Severance Hospital, Seoul, Korea, of the Yonsei University Health System [approval no. 4–2011–0872]) and adhered to the tenets of the Declaration of Helsinki.

FAP aptamer-functionalized hEV (hEV@FAP) were prepared by embedding cholesterol-conjugated FAP aptamer into human serum-derived EVs (hEV), as previously described.⁵⁴ Briefly, 0.5 µg/µL hEV in PBS was incubated with 1 µM cholesterol-conjugated FAP aptamer by ultrasonic soaking for 15 min. A Cy5.5-labeled scrambled (Scr) aptamer and FAP aptamer (with cholesterol conjugation) were synthesized by Aptamer Sciences (Seongnam, Korea). To remove unconjugated aptamers, hEV were washed twice with PBS using Amicon® Ultra Centrifugal Filters (UFC8010, Merck Millipore Ltd., Tullagreen, Ireland). hEV@FAP were resuspended, aliquoted, and stored at −80 °C.

Successful conjugation of the FAP aptamer to the hEV was assessed using the CD63 Exo-Flow Capture Kit (EXOFLOW300A-1, System Biosciences, Palo Alto, CA, USA) according to the manufacturer's instructions. Briefly, streptavidin-conjugated magnetic beads were mixed with a biotinylated anti-CD63 capture antibody on ice for 2 h, followed by overnight incubation with each EV sample on a rotating rack at 4 °C. To validate the isolation procedure, EV-coated beads were stained with Exo-FITC exosome stain on ice for 2 h and analyzed using a BD LSR II SORP Flow Cytometer (BD Biosciences, San Jose, CA, USA).

Scrambled siRNA (siCtrl) and TGFβ1 siRNA (siTGFβ1), synthesized by Bioneer (Daejeon, Korea), were loaded into hEV using the Exo-Fect™ Exosome Transfection kit (EXFT20A-1, System Biosciences) according to the manufacturer's instructions. Briefly, the hEV were mixed with Exo-Fect solution and 500 pmol of siCtrl or siTGFβ1 at 37 °C in a shaker for 10 min, incubated with 30 µL of ExoQuick-TC reagent on ice for 30 min, and centrifuged at 13,000 rpm for 3 min. To degrade unloaded siRNA, each EV sample was incubated with RNase A (12091021, Thermo Fischer Scientific) at 37 °C for 30 min, followed by two PBS washes using Amicon® Ultra Centrifugal Filters (UFC8010, Merck Millipore Ltd). In addition, FAM-labeled siCtrl-loaded hEV were solubilized in 0.5% Triton X-100 (93443, Sigma-Aldrich; Merck KGaA, Darmstadt, Germany), and fluorescence signals were detected to determine the concentration of siRNA loaded onto the hEV. A standard curve of free FAM-labeled siCtrl was used to calculate the siRNA concentration in the hEV.

Characterization of EVs

To observe the morphology of EVs, samples were placed on formvar carbon-coated electron microscopy grid (Leica Microsystems, Inc., Buffalo Grove, IL, USA) and stained with 2% uranyl acetate. The morphology of the EVs was then examined using transmission electron microscopy (TEM) (JEM-1011; JEOL Ltd., Tokyo, Japan).

Nanoparticle tracking analysis (NTA) was performed using a NanoSight LM10 instrument (Malvern Instruments Ltd., Malvern, UK). The Brownian motion of the EVs was captured for 60s at room temperature and analyzed using NTA v.2.3 software (Malvern Panalytical, Ltd.) based on the Stokes–Einstein equation.

The zeta potential of the EVs was evaluated to assess their surface charge. EVs were diluted to a 1:5,000 ratio in PBS and measured using an ELS-1000ZS instrument (Otsuka Electronics, Osaka, Japan).

Evaluation of Targeting Ability in vitro and in vivo

The cellular uptake of the EVs was evaluated in HEK293 cells using the BD™ LSR II SORP Flow Cytometer (BD Biosciences). Briefly, HEK293 cells transfected with GFP-tagged NC vector or GFP-tagged FAP expression vector were treated with respective EV samples for 24 h, washed twice with PBS, trypsinized, and centrifuged at 1,500 rpm for 5 min. The final pellet was resuspended in PBS and analyzed using BD FACSDiva™ Software.

For confocal microscopy, NC- or FAP-transfected HEK293 cells treated with each EV sample for 24 h were fixed with 4% paraformaldehyde for 20 min. After washing with PBS, the nuclei were stained with Hoechst 33342 (H3570, Thermo Fisher Scientific). Cells were observed under a confocal microscope (Zeiss LSM 710, Carl Zeiss, Oberkochen, Germany) and quantified using Zeiss ZEN (black edition) 3.0 SR.

To evaluate the in vivo distribution of the EVs, mice were intravenously injected with respective EV samples and euthanized 24 h post-injection. Cy 5.5 fluorescence intensity in dissected organs (heart, lung, spleen, kidneys, and liver) was detected using an IVIS® Spectrum in vivo imaging system (PerkinElmer, Waltham, MA, USA).

For histological analysis, cardiac tissues were cryosectioned 24 h post-injection and subjected to immunofluorescence staining with anti-FAP antibody (AF3715, R&D Systems, Minneapolis, MN, USA) and 4',6-diamidino-2-phenylindole (DAPI; 62248, Thermo Fisher Scientific). Stained slides were visualized using a confocal microscope (Zeiss LSM 710, Carl Zeiss).

Evaluation of Toxicity in vitro and in vivo

Cell viability and lactate dehydrogenase (LDH) release were evaluated using the Quint-MAX™ WST-8 Cell Viability Assay Kit (QM2500, Biomax, Seoul, Korea) and Quint-LDH™ PLUS Cytotoxicity Assay Kit (BCT-LDHP1000, Biomax) following the manufacturer's instructions. Absorbance was measured at 450 nm using a microplate reader (VersaMax, Molecular Devices, Sunnyvale, CA, USA).

To evaluate in vivo systemic toxicity, mice were intravenously injected with each EV sample. Twenty-four hours post-injection, various organs (heart, liver, spleen, lung, and kidneys) were dissected, fixed in 4% paraformaldehyde, embedded in paraffin, and sliced into 4-μm-thick sections. The sections were stained with hematoxylin and eosin (H&E) and observed under an inverted microscope (Olympus, Japan). In addition, serum biochemical parameters, including alanine aminotransferase (ALT), aspartate aminotransferase (AST), albumin (ALB), alkaline phosphatase (ALP), blood urea nitrogen (BUN), and creatinine (CRE), were measured using a Fuji Dri-Chem 4000i (Fujifilm, Tokyo, Japan) according to the manufacturer's instructions.

Quantitative Reverse Transcription Polymerase Chain Reaction (qRT-PCR)

Total RNA was extracted using the RNeasy® Mini Kit (74104, Qiagen, Hilden, Germany) and reverse-transcribed to cDNA using the High-Capacity cDNA Reverse Transcription Kit (4368814, Applied Biosystems, Darmstadt, Germany) following the manufacturer's instructions. qRT-PCR was performed on an AriaMx Real-time PCR System (Agilent Technologies, Santa Clara, CA, USA) using PowerUp™ SYBR™ Green Master Mix (A25742, Applied Biosystems). The relative mRNA expression levels were calculated according to the $2^{-\Delta\Delta C_q}$ method.⁵⁷ All primers were synthesized by Cosmo Genetech (Daejeon, Korea) and are listed in [Table S2](#).

Western Blotting Analysis

Total protein was extracted using radioimmunoprecipitation assay buffer containing protease and phosphatase inhibitors (WSE-7420, ATTO, Tokyo, Japan) and quantified using Pierce™ 660 nm Protein Assay Reagent (22660, Thermo Fisher Scientific). Equal amounts of protein were separated by 10% sodium dodecyl sulfate-polyacrylamide gel electrophoresis (SDS-PAGE) and transferred onto polyvinylidene fluoride membranes (IPVH00010, EMD Millipore, Bedford, MA, USA). After blocking with 5% bovine serum albumin (BSA) in TBS-Tween 20 (TBS-T) for 1 h, the membranes were incubated with the following primary antibodies: anti-TSG101 (sc-7964, 1:1,000; Santa Cruz Biotechnology Inc., Dallas, TX, USA), anti-CD81 (sc-166029, 1:1,000; Santa Cruz Biotechnology Inc.), anti-GRP94 (sc-393402, 1:1000; Santa Cruz Biotechnology Inc.), anti-FAP (AF3715, 1:500; R&D Systems), and GAPDH (sc-166574, 1:1,000; Santa Cruz Biotechnology Inc.). After overnight incubation at 4 °C, the membranes were incubated with horseradish peroxidase-conjugated secondary antibodies (sc-516102, sc-2357, 1:5,000; Santa Cruz Biotechnology Inc.) and visualized using an enhanced chemiluminescence kit (1705061, Bio-Rad Laboratories Inc., Hercules, CA, USA).

Animal Experiments

All animal experiments were performed in accordance with the procedures approved by the Institutional Animal Care and Use Committee of Yonsei University College of Medicine (approval no. 2023–0252) and the Guide for the Care and Use of Laboratory Animals published by the US National Institutes of Health (Publication No. 85–23, revised 1996). C57BL/6 mice were purchased from Orient Bio Inc. (Seongnam, Korea), maintained under standard conditions (temperature, 20 ± 0.5 °C; humidity, 60 ± 5%; light/dark cycle, 12 h), and allowed free access to food and water. To induce cardiac injury in vivo, the mice were anesthetized by intraperitoneal injections of tiletamine-zolazepam (Zoletil 50, 30 mg/kg) and xylazine (Rompun®, 10 mg/kg). They were then implanted with Ang II-containing Alzet® 1002 micro-osmotic pumps (1.5 mg/kg/day; Durect Corp., Cupertino, CA, USA). As a control, mice were implanted with PBS-containing Alzet® 1002 micro-osmotic pumps. After 7 days of implantation, mice were intravenously injected with each EV sample once every 2 days, after which organs (heart, liver, spleen, lung, and kidneys) were dissected for subsequent experiments.

To evaluate cardiac function, echocardiography was performed using a Vevo 2100 system (VisualSonics, Toronto, Ontario, Canada). The left ventricular ejection fraction (LVEF) and left ventricular fractional shortening (LVFS) were calculated as follows: $LVEF (\%) = [(left\ ventricle\ volume\ diastole\ (LV\ Vol;d) - Left\ ventricle\ volume\ systole\ (LV\ Vol;s)) / LV\ Vol;d] \times 100$; $LVFS (\%) = [(left\ ventricular\ internal\ diameter\ (diastole)\ (LVID;d) - left\ ventricular\ internal\ diameter\ (systole)\ (LVID;s)) / LVID;d] \times 100$.

To evaluate the fibrotic area and cross-sectional area (CSA), cardiac tissues were fixed in 4% paraformaldehyde, embedded in paraffin, sliced into 4- μ m thick sections, and stained with Masson's trichrome (MT) and Alexa Fluor 488-conjugated wheat germ agglutinin (WGA; W11261, Thermo Fisher Scientific), respectively. Five hearts were analyzed in each group and five individual fields were examined in each slide, resulting in the evaluation of 25 fields in total from each group. MT- and WGA-stained slides were observed under an inverted microscope (Olympus, Japan) and a confocal microscope (Zeiss LSM 710, Carl Zeiss), respectively. The fibrotic area and CSA were quantified using ImageJ 1.50i software (National Institutes of Health, Bethesda, MD, USA).

Immunohistochemical Analysis

To evaluate the expression of FAP, human and mouse cardiac tissues were deparaffinized, blocked with 5% BSA, and incubated with an anti-FAP antibody (AF3715, R&D Systems) overnight at 4 °C. Subsequently, all the specimens were incubated with fluorescent secondary antibodies (ab150177, Abcam, Cambridge, UK) for 1 h at room temperature. Nuclei were stained with DAPI (62248, Thermo Fisher Scientific). Slides were observed under a confocal microscope (Zeiss LSM 710, Carl Zeiss).

Human tissues were obtained from patients with and without heart failure (HF) during open-heart surgery at the Yonsei University Health System (Seoul, Korea) with informed consent. The clinical profiles of patients are presented in [Table S3](#). This study was approved by the local ethics committee (Institutional Review Board of Severance Hospital, Seoul, Korea, of the Yonsei University Health System [approval no. 4–2019–0620]) and adhered to the tenets of the Declaration of Helsinki.

Statistical Analyses

The data are presented as the mean \pm standard deviation. Statistical analyses were performed using a two-tailed Student's *t*-test for comparison between two groups and one-way analysis of variance with Tukey's post-hoc test for comparison involving multiple groups. All data were analyzed using GraphPad Prism (version 8.42, GraphPad, San Diego, CA, USA), and differences were considered statistically significant at $P < 0.05$.

Results

FAP Expression in Injured Cardiac Tissues

To identify a potential molecular target for targeted delivery to injured cardiac tissues, we first evaluated expression of FAP. As shown in [Figure 1A](#), qRT-PCR analysis revealed significantly increased FAP levels in the cardiac tissues of patients with HF compared to those without HF. Western blotting and immunofluorescence analyses further confirmed abundant FAP expression in the cardiac tissues of patients with HF ([Figure 1B–E](#)). Subsequently, mice were treated with Ang II for 2 weeks to establish a mouse model of cardiac injury. Ang II treatment resulted in a significant decline in cardiac function ([Figure S1](#)). Consistent with the FAP expression patterns observed in human tissues, FAP mRNA levels were also elevated in Ang II-treated mice compared to untreated controls ([Figure 1F](#)). Additionally, immunofluorescence staining revealed widespread distribution of FAP in the cardiac tissues of Ang II-treated mice ([Figure 1G and H](#)). Therefore, these findings suggest that the high expression of FAP in injured cardiac tissues makes it a suitable target for targeted delivery.

Preparation and Characterization of hEV@FAP

To develop EVs targeting injured cardiac tissues, we isolated EVs from human serum and functionalized them by embedding a cholesterol-conjugated FAP aptamer, which specifically targets FAP, as previously described ([Figure 2A](#)).⁵⁴

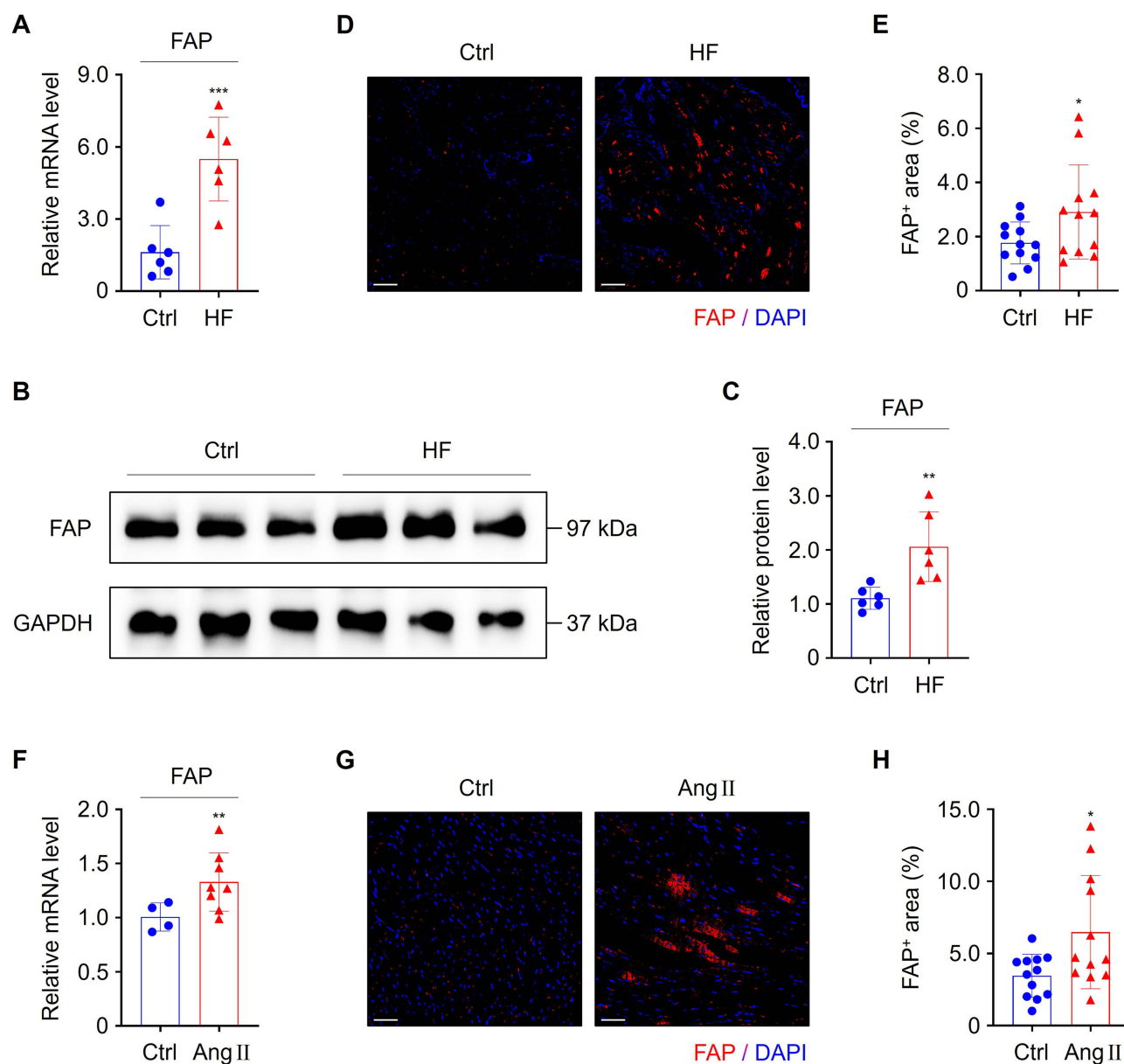


Figure 1 Expression of FAP in injured cardiac tissues. **(A)** qRT-PCR analysis of FAP levels in human cardiac tissues; $n = 6$ per group. Data are normalized to GAPDH. **(B and C)** Representative blots and quantified data showing FAP levels in the indicated groups. GAPDH served as a loading control. Uncropped blots are shown in [Figure S7](#). **(D and E)** Representative immunofluorescence images of FAP (red)- and DAPI (blue)-stained cardiac tissue sections and quantified data showing FAP-positive areas (%). **(F)** qRT-PCR analysis of FAP levels in cardiac tissues of untreated ($n = 4$) and Ang II-treated mice ($n = 8$). Data are normalized to GAPDH. **(G and H)** Representative immunofluorescence images of FAP (red)- and DAPI (blue)-stained cardiac tissue sections and quantified data showing FAP-positive areas (%). Scale bar = 50 μm . * $P < 0.05$, ** $P < 0.01$, *** $P < 0.001$.

The resulting FAP aptamer-functionalized EVs were named hEV@FAP. As a control, we prepared Scr aptamer-embedded hEV (hEV@Scr). Flow cytometry analysis of hEV incubated with different concentrations of Cy5.5-labeled FAP aptamer (with cholesterol conjugation) for 15 min indicated that the modification efficiency was increased with the FAP aptamer concentration, plateauing at 1 μM ([Figure 2B](#)). Based on this optimal modification efficiency, hEVs were incubated with 1 μM FAP aptamer, resulting in hEV@FAP with a positive rate of $>80\%$. Therefore, these results confirmed the successful conjugation of the FAP aptamer to the surface of the hEV.

After preparing hEV@FAP, we performed TEM, NTA, Western blotting, and electrophoretic light scattering (ELS) to characterize their morphology, diameter, marker protein expression, and zeta potential of the EVs, respectively. TEM analysis revealed that all three types of EVs exhibited typical round, cup-shaped vesicles ([Figure 2C](#)). NTA results

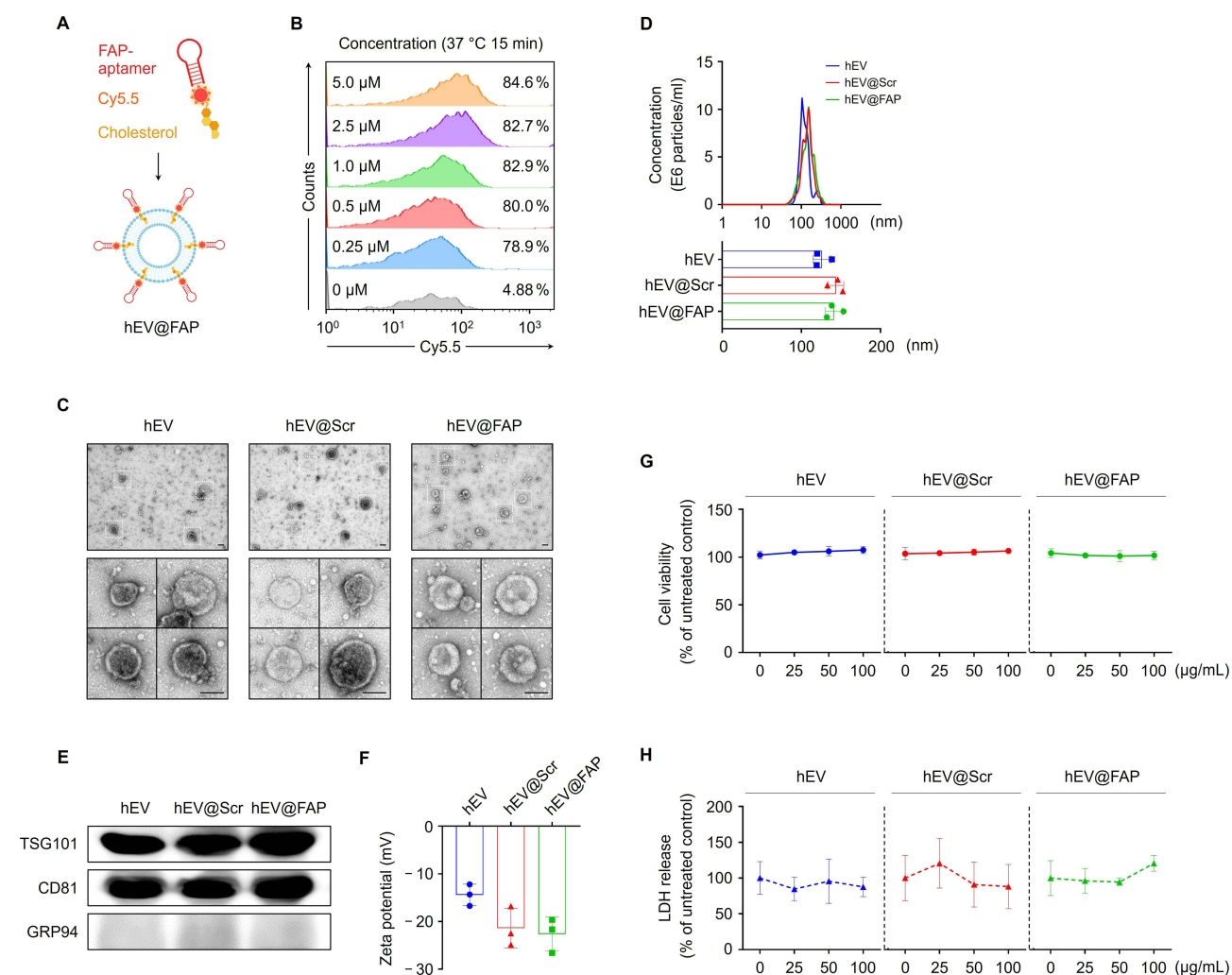


Figure 2 Characterization of hEV@FAP and its toxicity in vitro. (A) Schematic illustration of hEV@FAP preparation by embedding a cholesterol-conjugated FAP aptamer onto the hEV. Cy5.5-labeled FAP aptamer was conjugated to visualize the surface modification of hEV@FAP. (B) Representative flow cytometric images of the modification efficiency of Cy5.5-labeled FAP aptamer with different concentrations on the hEV. (C) Transmission electron micrograph of hEV, hEV@Scr, and hEV@FAP. Scale bar = 100 nm. (D) Size distribution of hEV, hEV@Scr, and hEV@FAP. (E) Representative blots of TSG101, CD81, and GRP94 in three types of EVs. Uncropped blots are shown in Figure S7. (F) Zeta potential analysis of hEV, hEV@Scr, and hEV@FAP. (G and H) The analysis of cell viability and LDH release in HEK293 cells treated with hEV, hEV@Scr, or hEV@FAP.

showed that the diameters of the EVs were predominantly in the range of 100 to 200 nm, with mean diameters of 126.0 ± 6.3 nm for hEV, 143.7 ± 5.7 nm for hEV@Scr, and 141.4 ± 6.2 nm for hEV@FAP (Figure 2D). Western blotting analysis confirmed that all EVs abundantly expressed EV-specific markers, such as TSG101 and CD81, while GRP94, a known endoplasmic reticulum marker, was absent (Figure 2E). As shown in Figure 2F, the zeta potentials of all three EVs were negative, at -14.4 ± 1.3 mV for hEV, -21.4 ± 2.4 mV for hEV@Scr, and -22.6 ± 2.1 mV for hEV@FAP. Therefore, these results demonstrate that typical EV properties were maintained following the surface modification of hEV by conjugation with the FAP aptamer. In addition, toxicity assays were conducted in vitro using cell viability and LDH release assays. Incubation of each EV sample with HEK293 cells did not induce observable toxicity within the 100 μ g/mL concentration range (Figure 2G and H). Moreover, there were no significant changes in the mean diameter of hEV@FAP after storage at 4 °C for 7 days or at -80 °C for 4 weeks (Figure S2). Collectively, these results indicate that hEV@FAP could potentially be used in subsequent experiments without compromising its properties or stability.

Targeting Capability of hEV@FAP in vitro and in vivo

To evaluate the targeting specificity of hEV@FAP for FAP in vitro, we first generated HEK293 cells with high FAP expression by transfecting them with a GFP-tagged FAP expression vector. Control HEK293 cells were transfected with a GFP-tagged NC vector. After 24 h of incubation with each EV sample, flow cytometry analysis showed that FAP-transfected HEK293 cells internalized significantly more hEV@FAP than hEV@Scr. In contrast, no significant difference in EV uptake was observed between hEV@Scr and hEV@FAP in NC-transfected HEK293 cells (Figure 3A and B). Similarly, immunofluorescence analysis revealed that hEV@FAP was preferentially internalized by FAP-transfected HEK293 cells, confirming the FAP aptamer's ability to selectively target FAP (Figure 3C and D). Therefore, these results indicate that hEV@FAP selectively targets FAP-positive areas in vitro.

In vivo distribution of hEV@FAP was evaluated in Ang II-treated mice using an IVIS® Spectrum in vivo imaging system. After 24 h of intravenous injection with each EV sample, fluorescence intensity was significantly higher in the injured cardiac tissues of hEV@FAP-injected mice compared to hEV@Scr-injected mice (fold change ≥ 1.5 , $P < 0.05$; Figure 3E and F). However, no significant differences in fluorescence intensity were observed in other organs (lung, spleen, kidneys, and liver) between the two groups (Figure S3). Of note, neither type of EV treatment affected the fluorescence intensity of different organs (heart, lung, spleen, kidneys, and liver) in untreated normal mice (Figure S4).

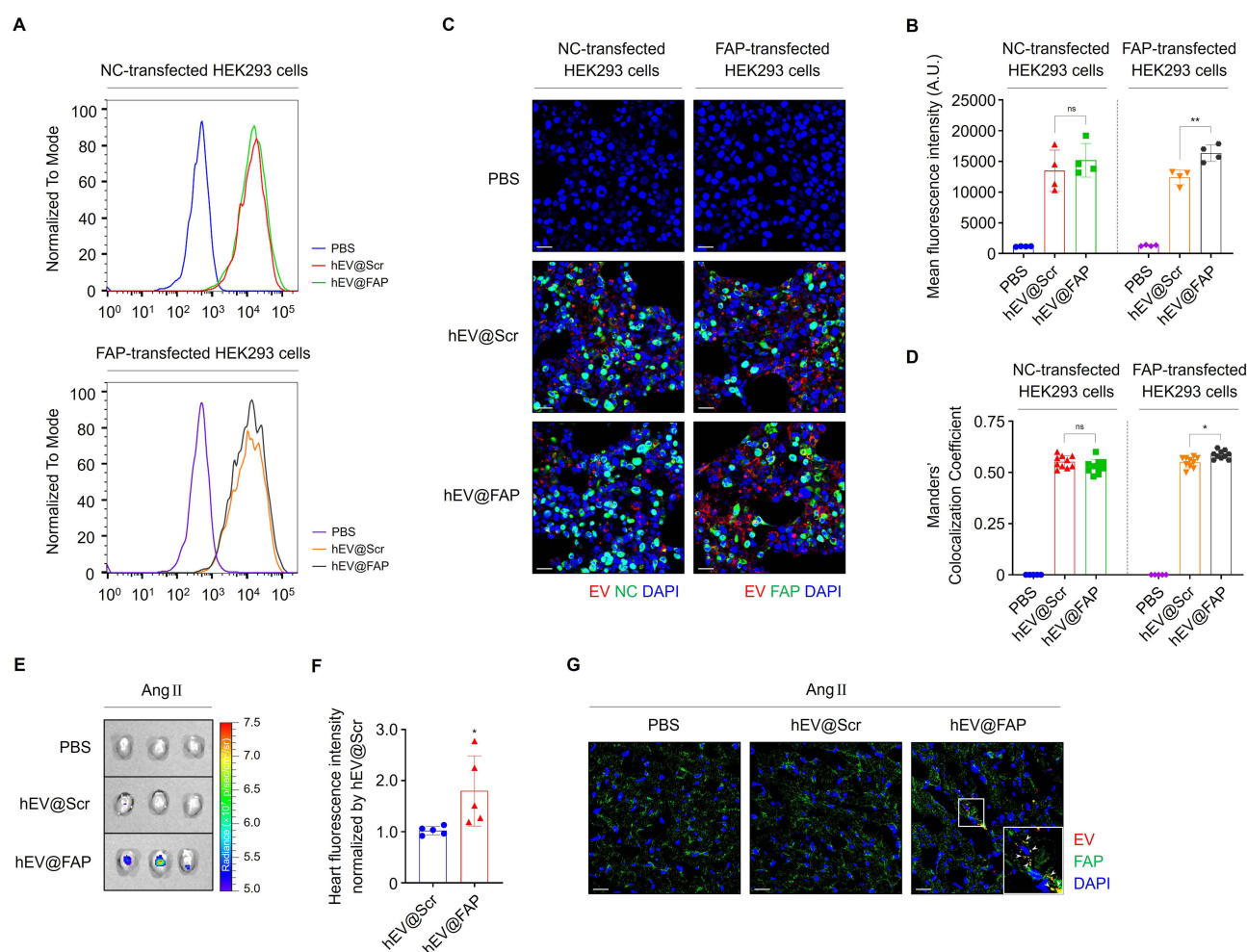


Figure 3 In vitro and in vivo targeting selectivity of hEV@FAP. **(A and B)** Representative flow cytometric images and quantified data showing cellular uptake of Cy5.5 (red)-labeled hEV@Scr and hEV@FAP by HEK293 cells transfected with GFP-tagged NC vector or GFP-tagged FAP expression vector. **(C and D)** Representative immunofluorescence images and quantified data showing NC- or FAP-transfected HEK293 cells (green). Nuclei were stained with Hoechst 33342 (blue). Red fluorescence indicates Cy5.5-labeled aptamer-conjugated hEV. Scale bar = 50 μ m. **(E and F)** Representative IVIS images and quantified data showing the fluorescence intensity in the cardiac tissues of Ang II-treated mice at 24 h after intravenous injection of PBS, hEV@Scr, or hEV@FAP; $n = 5$ per group. **(G)** Representative immunofluorescence images of PBS, hEV@Scr, and hEV@FAP accumulated in FAP-positive areas. Nuclei were stained with DAPI (blue); $n = 5$ per group. Scale bar = 20 μ m. * $P < 0.05$, ** $P < 0.01$.

Subsequently, the cell distribution of hEV@FAP was investigated by immunofluorescence staining of frozen cardiac tissue sections. As shown in [Figure 3G](#), hEV@FAP were abundantly accumulated in FAP-positive areas compared to hEV@Scr. Collectively, these results demonstrate that hEV@FAP preferentially targets FAP in injured cardiac tissues, highlighting its potential as an effective delivery system for targeting injured cardiac tissues.

Characterization of hEV@FAP-siTGFβ1 and Its Functionality

To investigate whether hEV@FAP could successfully deliver siRNA and exert cardioprotective effects, we first selected a suitable siRNA candidate. Previous studies have demonstrated overexpression of TGFβ1 during cardiac remodeling, including fibrosis and hypertrophy, in injured cardiac tissues, eventually leading to cardiac dysfunction.^{58–60} Therefore, inhibiting TGFβ1 expression is considered a potential approach for cardiac repair. Schultz et al⁶¹ demonstrated that TGFβ1 knockout mice experienced significantly alleviated pathological cardiac hypertrophy induced by Ang II. In addition, recent studies have found that the inhibition of TGFβ1 attenuates progressive worsening of cardiac structure and function by blocking TGFβ1-mediated phosphorylation of Smad2/3.^{62–64}

Given these findings, we hypothesized that hEV@FAP-mediated delivery of siTGFβ1 could exert strong cardioprotective effects. Consequently, siTGFβ1-loaded hEV@FAP were generated as previously described ([Figure 4A](#)).⁶⁵ Using a fluorescence standard curve for free FAM-labeled siCtrl, it was determined that 100 µg/mL of siCtrl-loaded hEV contained an average of 342 pmol siRNA ([Figure S5](#)). Given that 100 µg/mL of the hEV was initially incubated with 500 pmol siRNA, the loading efficiency was approximately 68.4%. As shown in [Figure 4B–E](#), there were no changes in the morphology, diameter, marker protein expression levels, or zeta potential of hEV@FAP-siTGFβ1, confirming that typical EV properties were not affected following loading of siTGFβ1. Additionally, to assess the specificity of siRNA delivery, we examined whether hEV@FAP could target FAP-expressing cells. In FAP-transfected HEK293 cells, treatment with hEV@FAP-siTGFβ1 significantly decreased TGFβ1 mRNA levels compared to its levels in cells treated with hEV@FAP-siCtrl or hEV@Scr-siTGFβ1, indicating dependence on targeted delivery to FAP-positive areas by hEV@FAP ([Figure 4F](#)). Similar to the in vitro results, an increase in Cy5.5 fluorescence intensity was detected in injured cardiac tissues from Ang II-treated mice 24 h after intravenous injection of hEV@FAP-siCtrl or hEV@FAP-siTGFβ1, suggesting that the FAP aptamer can specifically redirect the systemic distribution of hEV to injured cardiac tissues ([Figure 4G and H](#)). However, no significant differences in the fluorescence intensity were detected in other organs, including, the lung, spleen, kidneys, and liver ([Figure S6](#)). Collectively, these results demonstrate that hEV@FAP efficiently encapsulates siTGFβ1 and successfully delivers it to target areas.

Targeted Therapy of hEV@FAP-siTGFβ1 in vivo

To examine the in vivo cardioprotective effects of hEV@FAP-siTGFβ1, Ang II-treated mice were intravenously injected with each EV sample, as shown in [Figure 5A](#). qRT-PCR analysis revealed that the Ang II-treated group exhibited markedly elevated TGFβ1 levels compared to the control group. However, these changes were significantly reversed following hEV@FAP-siTGFβ1 injection, indicating successful delivery of siTGFβ1 to injured cardiac tissues of mice ([Figure 5B](#)). Consequently, histological analysis showed a significant reduction in the Ang II-induced fibrotic area and cell CSA in the hEV@FAP-siTGFβ1-injected group compared to those injected with hEV@FAP-siCtrl or hEV@Scr-siTGFβ1 ([Figure 5C–F](#)). In addition, echocardiography results showed that Ang II treatment led to deterioration of cardiac function (LVEF, LVFS, LVID;d, and LVID;s); however, hEV@FAP-siTGFβ1 injection resulted in a more pronounced improvement in cardiac function relative to the other two groups ([Figure 5G and H](#)). As shown in [Figure 5I](#), the hEV@FAP-siTGFβ1-injected group showed significantly decreased Ang II-induced levels of collagen I and collagen III, which are known as markers of myocardial fibrosis ($P < 0.05$). Moreover, Ang II treatment significantly increased the mRNA levels of hypertrophic markers (ANP and BNP), whereas these changes were reversed following hEV@FAP-siTGFβ1 injection compared to the levels in mice injected with hEV@FAP-siCtrl or hEV@Scr-siTGFβ1 ([Figure 5J](#)). Taken together, these results show that hEV@FAP-siTGFβ1 exerts a stronger protective effect against cardiac injury, which can be attributed to the targeted delivery of siTGFβ1 to injured cardiac tissues.

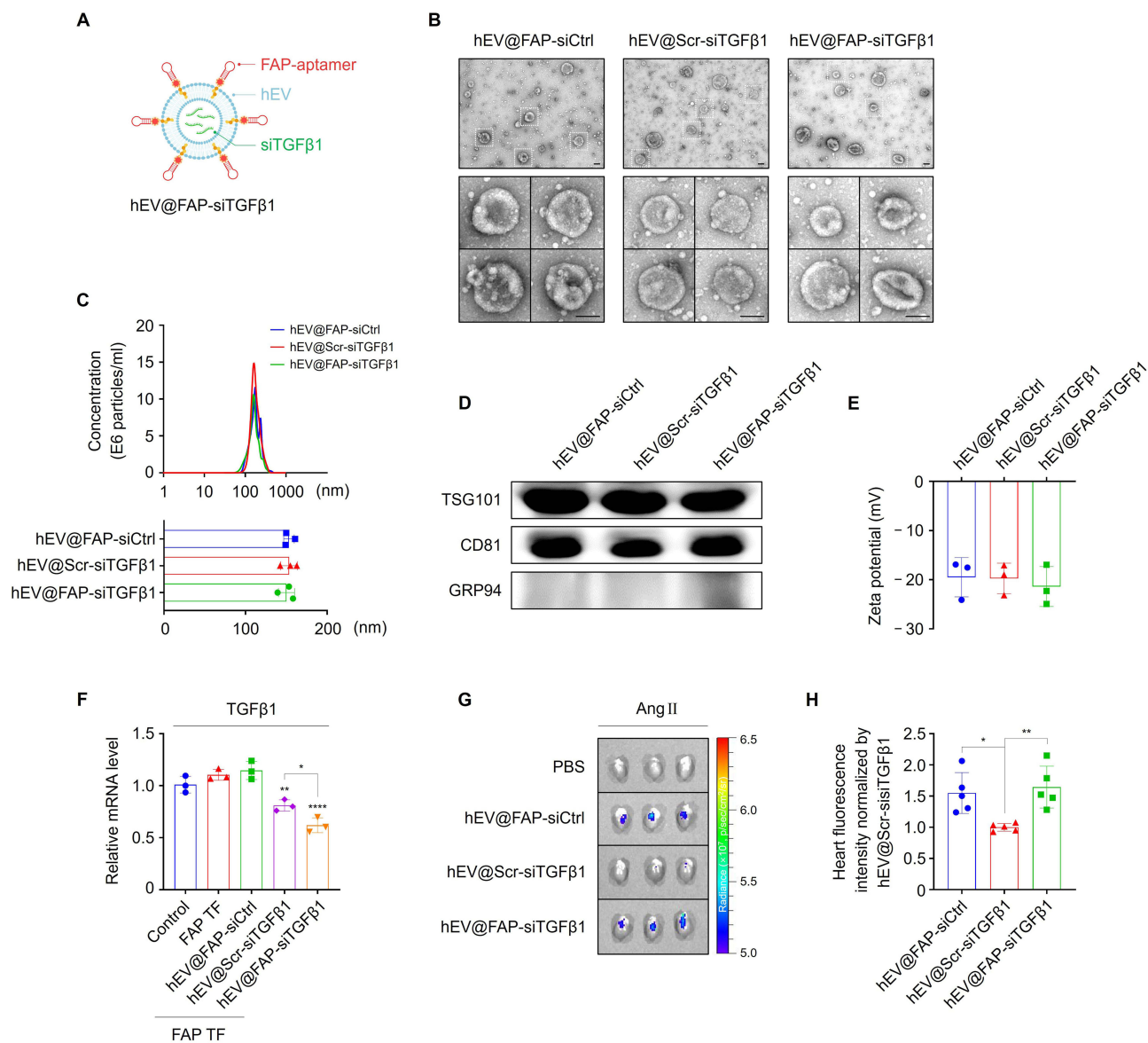


Figure 4 Preparation and characterization of hEV@FAP-siTGFβ1. **(A)** Schematic illustration showing generation of siTGFβ1-loaded hEV@FAP. **(B and C)** Transmission electron micrograph **(B)** and size distribution **(C)** of hEV@FAP-siCtrl, hEV@Scr-siTGFβ1, and hEV@FAP-siTGFβ1. Scale bar = 100 nm. **(D)** Representative blots of TSG101, CD81, and GRP94 in three types of EVs. Uncropped blots are shown in [Figure S7](#). **(E)** Zeta potential analysis of hEV@FAP-siCtrl, hEV@Scr-siTGFβ1, and hEV@FAP-siTGFβ1. **(F)** qRT-PCR analysis of TGFβ1 levels in the indicated groups. Data are normalized to GAPDH. **(G and H)** Representative IVIS images and quantified data showing the fluorescence intensity in the cardiac tissues of Ang II-treated mice at 24 h after intravenous injection of PBS, hEV@FAP-siCtrl, hEV@Scr-siTGFβ1, or hEV@FAP-siTGFβ1; n = 5 per group. **P* < 0.05, ***P* < 0.01, ****P* < 0.0001. FAP TF = FAP-transfected HEK293 cells.

In vivo Safety of hEV@FAP-siTGFβ1

The systemic toxicity of hEV@FAP-siTGFβ1 was further evaluated *in vivo*. Histological examination of major organs, including the heart, liver, spleen, lung, and kidneys, revealed no noticeable changes or damage in H&E-stained sections following intravenous injection of each EV sample ([Figure 6A](#)). In addition, the treatment did not affect the levels of key biochemical parameters, including ALT, AST, ALB, ALP, BUN, and CRE ([Figure 6B–G](#)). Therefore, these results suggest that hEV@FAP can potentially be used as a safe nanocarrier for siRNA delivery, thereby supporting its potential clinical application in the treatment of cardiac injury.

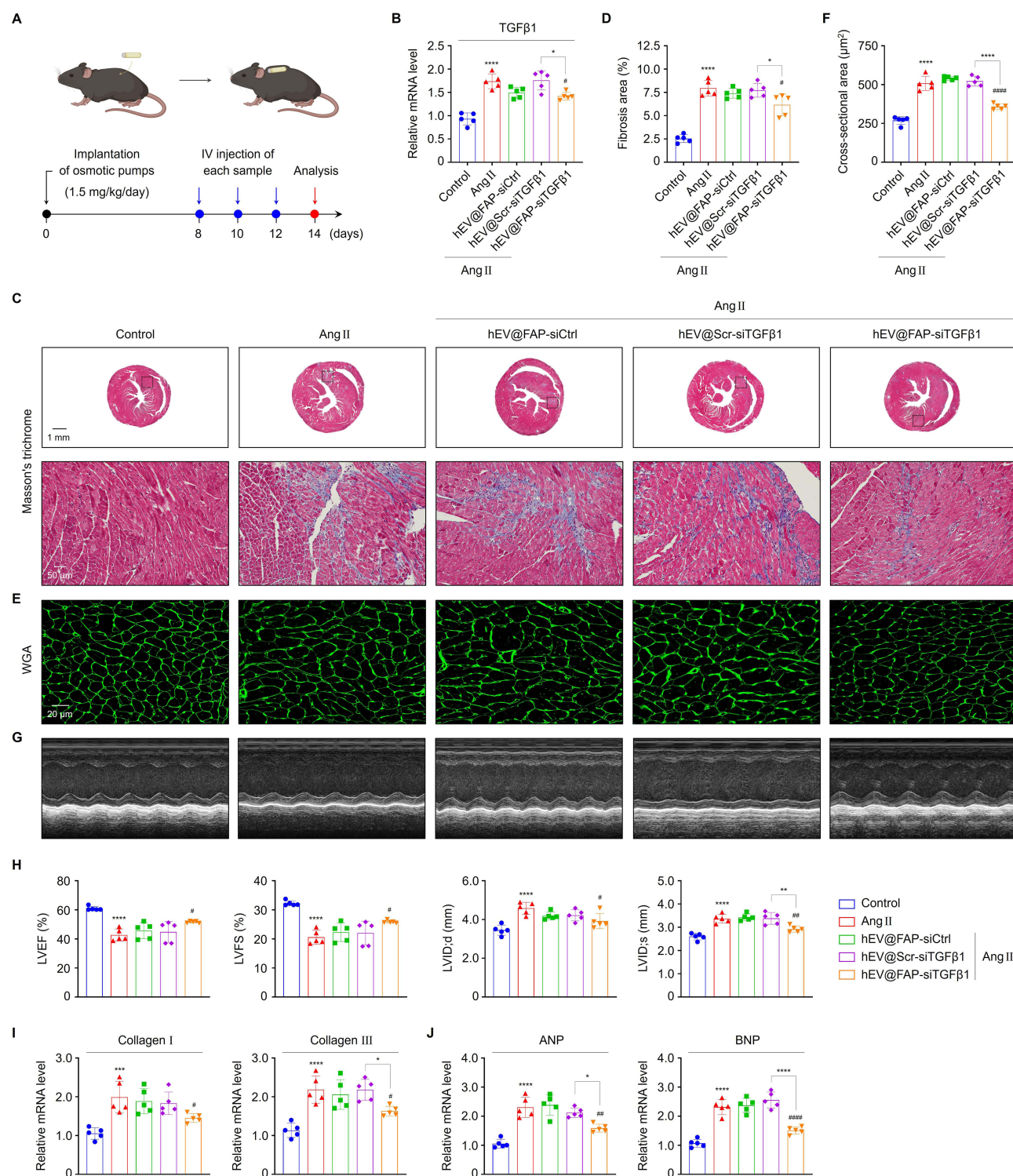


Figure 5 Therapeutic effects of hEV@FAP-siTGFβ1 in vivo. **(A)** Schematic illustration of in vivo experimental procedure. **(B)** qRT-PCR analysis of TGFβ1 levels in the cardiac tissues of mice; n = 5 per group. Data are normalized to GAPDH. **(C and D)** Representative images of MT-stained cardiac sections at low (× 12.5) to high (× 200) magnification and quantified data showing fibrotic area (%); n = 5 per group. Scale bar = 1 mm (top row) and 50 μm (bottom row). **(E and F)** Representative immunofluorescence images of WGA-stained cardiac sections and quantified data showing CSA; n = 5 per group. Scale bar = 20 μm. **(G and H)** Representative M-mode images **(G)** and quantified data showing LVEF, LVFS, LVID:d, and LVID:s **(H)** in the indicated groups; n = 5 per group. **(I and J)** qRT-PCR analysis of collagen I, collagen III, ANP, and BNP levels in the indicated groups; n = 5 per group. Data are normalized to GAPDH. *indicates comparison with the control group, *P < 0.05, **P < 0.01, ***P < 0.001, ****P < 0.0001; # indicates comparison with the Ang II-treated group, #P < 0.05, ##P < 0.01, ###P < 0.0001.

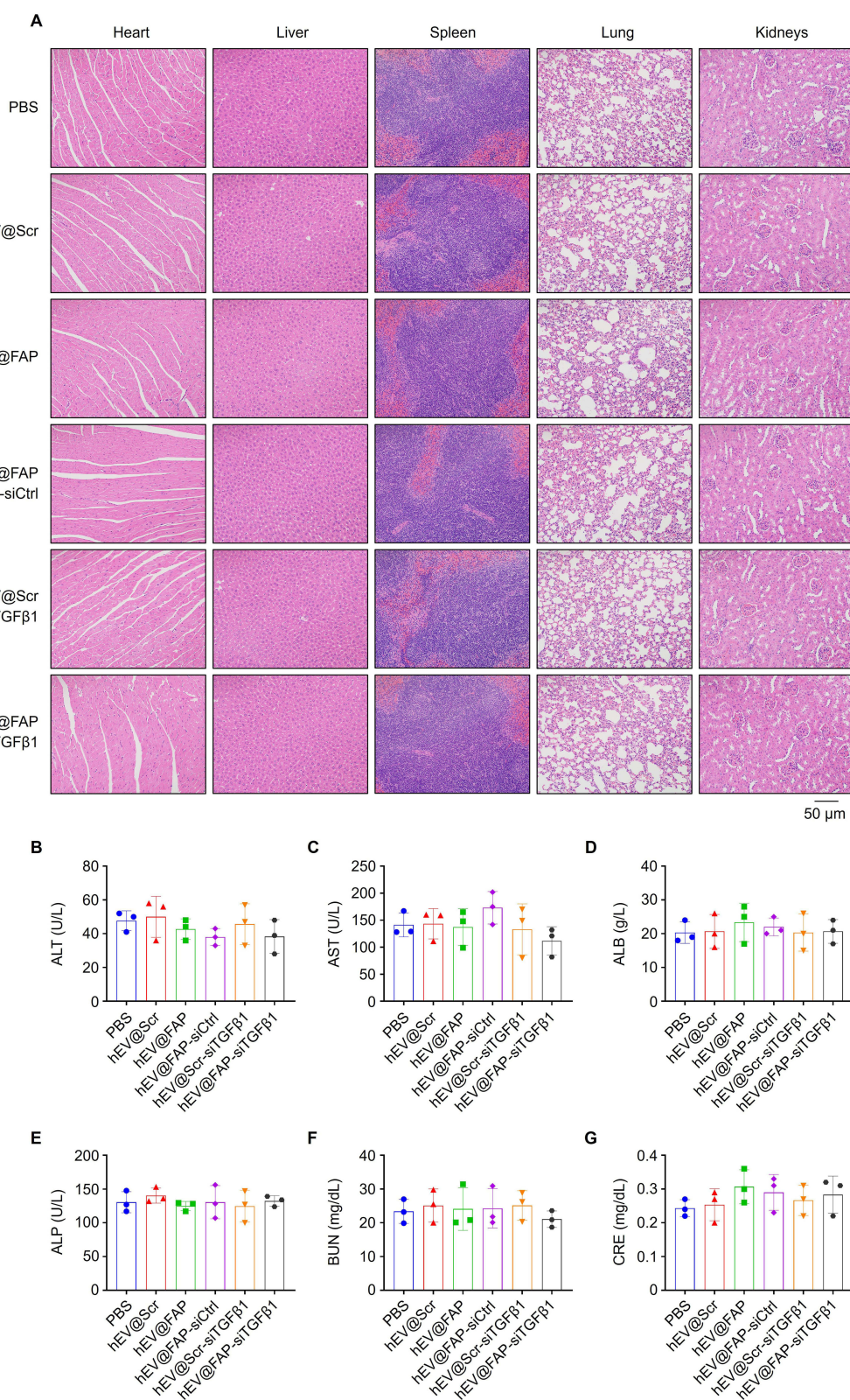


Figure 6 Biosafety of hEV@FAP-siTGFB1 in vivo. **(A)** Representative images of H&E-stained different organs (heart, liver, spleen, lung, and kidneys) at 24 h after intravenous injection of PBS, hEV@Scr, hEV@FAP, hEV@FAP-siCtrl, hEV@Scr-siTGFB1, or hEV@FAP-siTGFB1; n = 3 per group. Scale bar = 50 μ m. **(B–G)** The levels of ALT, AST, ALB, ALP, BUN, and CRE in serum of mice at 24 h after intravenous injection of each EV sample; n = 3 per group.

Discussion

In this study, we developed an EV-based nanoplatform for the targeted delivery of therapeutic siRNA to injured cardiac tissue, aiming to facilitate cardiac repair. EVs, with their inherent biocompatibility as a natural ability to serve as carriers, offer distinct advantages, including robust cargo-loading capacity and modifiable surface properties. These features allow for the integration of tissue-specific targeting moieties and therapeutic siRNA into a single EV while preserving their respective functionalities. Consequently, EVs hold considerable potential as siRNA delivery systems to treat cardiac injuries.^{42–44} However, unmodified EVs face notable limitations when administered systemically, such as non-specific accumulation in tissues, especially in the liver, and rapid clearance by macrophages.^{40,41} To overcome these challenges, we modified hEV with the FAP aptamer to enable selective targeting of FAP, which is abundantly expressed in injured cardiac tissues and serves as an ideal target for site-specific delivery. Our in vitro and in vivo results validated the high targeting capability of hEV@FAP to FAP-positive areas, highlighting its potential as an effective delivery system for targeting injured cardiac tissues.

Low yields of EVs remain a significant challenge for advancing research and clinical applications.^{66–68} Studies have shown that EV yields from cell culture media are typically low, often requiring billions of cells to produce sufficient EVs.^{66,67} This limitation is further exacerbated when using primary cells, which are not easy to culture.⁶⁷ Interestingly, cell-derived nanovesicles (CDNs) have emerged as a promising alternative to EVs due to their high productivity and their biochemical, structural, and functional similarities to natural EVs.^{69,70} Unlike EVs harvested from conditioned media, CDNs are artificially synthesized from living cells using physical methods, such as serial extrusion through porous membrane filters.⁶⁹ Among these, cancer cell-derived CDNs are being extensively investigated for their therapeutic potential, cancer-homing capabilities, and high production efficiency.^{69,71} However, the use of cancer cell-derived CDNs raises safety concerns, particularly the potential transfer of oncogenic DNA and retrotransposon elements.⁷² In contrast, human serum can be easily obtained from any individual and has been routinely and safely used in blood transfusions. Accumulating evidence indicates that hEV can serve as effective nanocarriers with minimal risk of toxicity or immunogenicity in animal models, including mice and rats.^{67,73–75} Therefore, we selected human serum as the source of EV production in this study. The resulting hEV@FAP system represents an efficient and safe delivery platform for siRNA, addressing the dual challenges of low EV yield and potential safety concerns associated with other vesicle production methods.

Recent studies have shown that inhibiting TGF β 1 levels in injured cardiac tissues promotes cardiac repair,^{58,62–64} making it a promising therapeutic strategy for treating cardiac injury. Therefore, we encapsulated siTGF β 1 within hEV@FAP to enhance its therapeutic efficacy for cardiac repair. The siTGF β 1 encapsulation within hEV@FAP provides protection and ensures targeted delivery to injured cardiac tissues. As a result, intravenous injection of hEV@FAP-siTGF β 1 led to a significant decrease in Ang II-induced TGF β 1 levels and exerted strong cardioprotective effects in Ang II-treated mice. Therefore, hEV@FAP-mediated delivery of siTGF β 1 may potentially be used for the treatment of cardiac injury. Given FAP's role in tissue remodeling and its high expression in fibrotic conditions involving the liver, lung, and colon, as well as peri-tumoral tissue,^{76,77} hEV@FAP represents a versatile platform for delivering therapeutic siRNA to FAP-positive areas in various diseases. Additionally, in cases involving comorbidities, localized or regional administration of hEV@FAP may offer a more suitable and targeted approach, potentially achieving improved therapeutic outcomes.

The present study has several limitations. First, considering that a higher zeta potential in hEV increases the likelihood of aggregation, which could compromise their functional stability in circulation,⁷⁸ future research should focus on additional modifications of hEV to optimize their zeta potential. In addition, local or regional delivery methods could help address concerns with aggregation and enhance therapeutic efficiency in clinical settings. Second, we did not directly investigate how EVs selectively improve RNA delivery; thus, further studies are needed to understand the mechanisms by which EVs enter target cells, escape from endosomes, and deliver their cargo, which could provide deeper insights into EV-based delivery systems. Third, the functionality of the developed EVs was not evaluated in vitro using primary cardiac cells in this study. Additionally, there is a lack of validation regarding the impact of FAP manipulation on various mechanisms, including cardiac regeneration. Therefore, further investigation into its functional roles in cardiac repair using an in vitro cardiac injury model with primary cardiac fibroblasts or smooth muscle cells could expand its potential as a target for genetic or pharmacological interventions.

Conclusion

In summary, the development of hEV@FAP represents a novel and effective strategy for targeted delivery of therapeutic siRNA to injured cardiac tissues, demonstrating significant potential for promoting cardiac repair. Our findings not only suggest a practical strategy to overcome obstacles for siRNA delivery but also provide a promising avenue for efficient and tissue-specific siRNA therapy to treat cardiac injury, with the potential to be extended for the treatment of various FAP-associated diseases.

Data Sharing Statement

The datasets used and/or analyzed during the current study are available from the corresponding author on reasonable request.

Ethics Approval and Consent to Participate

This study was approved by the local ethics committee (Institutional Review Board of Severance Hospital, Seoul, Korea, of the Yonsei University Health System [approval no. 4–2011–0872 and 4–2019–0620]) and adhered to the tenets of the Declaration of Helsinki. All animal experiments were performed in accordance with the procedures approved by the Institutional Animal Care and Use Committee of Yonsei University College of Medicine (approval no. 2023–0252) and the Guide for the Care and Use of Laboratory Animals published by the US National Institutes of Health (Publication No. 85–23, revised 1996).

Acknowledgments

This study was supported by the Korean Fund for Regenerative Medicine (KFRM), funded by the Ministry of Science and ICT and Ministry of Health and Welfare (21B0604L1 and 24A0202L1); the Basic Science Research Program through National Research Foundation of Korea (NRF) funded by the Ministry of Education (2021R1I1A1A01052197); the NRF grant funded by the Ministry of Science and ICT (2023R1A2C3003320); and the Korean Cardiac Research Foundation (202101-02). The authors would like to thank Editage (www.editage.co.kr) for English language editing and BioRender (www.biorender.com) for assistance with figure preparation.

Disclosure

The authors declare that they have no conflicts of interest in this work.

References

1. Frangogiannis NG. The inflammatory response in myocardial injury, repair, and remodelling. *Nat Rev Cardiol.* 2014;11(5):255–265. doi:10.1038/nrcardio.2014.28
2. Epelman S, Liu PP, Mann DL. Role of innate and adaptive immune mechanisms in cardiac injury and repair. *Nat Rev Immunol.* 2015;15(2):117–129. doi:10.1038/nri3800
3. Hashimoto H, Olson EN, Bassel-Duby R. Therapeutic approaches for cardiac regeneration and repair. *Nat Rev Cardiol.* 2018;15(10):585–600. doi:10.1038/s41569-018-0036-6
4. Rurik JG, Aghajanian H, Epstein JA. Immune Cells and Immunotherapy for Cardiac Injury and Repair. *Circulation Research.* 2021;128(11):1766–1779. doi:10.1161/CIRCRESAHA.121.318005
5. Han M, Zhou B. Role of Cardiac Fibroblasts in Cardiac Injury and Repair. *Curr Cardiol Rep.* 2022;24(3):295–304. doi:10.1007/s11886-022-01647-y
6. Ponikowski P, Anker SD, AlHabib KF, et al. Heart failure: preventing disease and death worldwide. *ESC Heart Fail.* 2014;1(1):4–25. doi:10.1002/ehf2.12005
7. Sapna F, Raveena F, Chandio M, et al. Advancements in Heart Failure Management: a Comprehensive Narrative Review of Emerging Therapies. *Cureus.* 2023;15(10):e46486. doi:10.7759/cureus.46486
8. McManus MT, Sharp PA. Gene silencing in mammals by small interfering RNAs. *Nat Rev Genet.* 2002;3(10):737–747. doi:10.1038/nrg908
9. Lefer DJ. Induction of HIF-1 α and iNOS with siRNA: a novel mechanism for myocardial protection. *Circulation Research.* 2006;98(1):10–11. doi:10.1161/01.RES.0000200398.52220.cc
10. Poller W, Tank J, Skurk C, Gast M. Cardiovascular RNA interference therapy: the broadening tool and target spectrum. *Circulation Research.* 2013;113(5):588–602. doi:10.1161/CIRCRESAHA.113.301056
11. Chen L, Zhang D, Yu L, Dong H. Targeting MIAT reduces apoptosis of cardiomyocytes after ischemia/reperfusion injury. *Bioengineered.* 2019;10(1):121–132. doi:10.1080/21655979.2019.1605812
12. Shah AM, Giacca M. Small non-coding RNA therapeutics for cardiovascular disease. *Eur Heart J.* 2022;43(43):4548–4561. doi:10.1093/eurheartj/ehac463
13. Reischl D, Zimmer A. Drug delivery of siRNA therapeutics: potentials and limits of nanosystems. *Nanomedicine.* 2009;5(1):8–20. doi:10.1016/j.nano.2008.06.001

14. Wang J, Lu Z, Wientjes MG, Au JL. Delivery of siRNA therapeutics: barriers and carriers. *AAPS J.* 2010;12(4):492–503. doi:10.1208/s12248-010-9210-4
15. Moazzam M, Zhang M, Hussain A, Yu X, Huang J, Huang Y. The landscape of nanoparticle-based siRNA delivery and therapeutic development. *Mol Ther.* 2024;32(2):284–312. doi:10.1016/j.ymthe.2024.01.005
16. Kanasty R, Dorkin JR, Vegas A, Anderson D. Delivery materials for siRNA therapeutics. *Nat Mater.* 2013;12(11):967–977. doi:10.1038/nmat3765
17. Tatiparti K, Sau S, Kashaw SK, Iyer AK. siRNA Delivery Strategies: a Comprehensive Review of Recent Developments. *Nanomaterials.* 2017;7(4):77. doi:10.3390/nano7040077
18. Mamidi N, Delgadillo RMV, Barrera EV, Ramakrishna S, Annabi N. Carbonaceous nanomaterials incorporated biomaterials: the present and future of the flourishing field. *Compos Part B-Eng.* 2022;243:110150.
19. Sana SS, Hou TY, Li HZ, et al. Crude Polysaccharide Produces Silver Nanoparticles with Inherent Antioxidant and Antibacterial Activity. *Chemistryselect.* 2023;8(18). doi:10.1002/slct.202203658.
20. Hou T, Sankar Sana S, Li H, et al. Development of Plant Protein Derived Tri Angular Shaped Nano Zinc Oxide Particles with Inherent Antibacterial and Neurotoxicity Properties. *Pharmaceutics.* 2022;14(10):2155. doi:10.3390/pharmaceutics14102155
21. Zu H, Gao D. Non-viral Vectors in Gene Therapy: recent Development, Challenges, and Prospects. *AAPS J.* 2021;23(4):78. doi:10.1208/s12248-021-00608-7
22. Colombo M, Raposo G, Thery C. Biogenesis, secretion, and intercellular interactions of exosomes and other extracellular vesicles. *Annu Rev Cell Dev Biol.* 2014;30(1):255–289. doi:10.1146/annurev-cellbio-101512-122326
23. Shah R, Patel T, Freedman JE. Circulating Extracellular Vesicles in Human Disease. *N Engl J Med.* 2018;379(10):958–966. doi:10.1056/NEJMr1704286
24. S ELA, Mager I, Breakefield XO, Wood MJ. Extracellular vesicles: biology and emerging therapeutic opportunities. *Nat Rev Drug Discov.* 2013;12(5):347–357. doi:10.1038/nrd3978
25. Sahoo S, Adamiak M, Mathiyalagan P, Kenneweg F, Kafert-Kasting S, Thum T. Therapeutic and Diagnostic Translation of Extracellular Vesicles in Cardiovascular Diseases: roadmap to the Clinic. *Circulation.* 2021;143(14):1426–1449. doi:10.1161/CIRCULATIONAHA.120.049254
26. Zhang Y, Liu Y, Liu H, Tang WH. Exosomes: biogenesis, biologic function and clinical potential. *Cell Biosci.* 2019;9(1):19. doi:10.1186/s13578-019-0282-2
27. Xu R, Rai A, Chen M, Suwakulsiri W, Greening DW, Simpson RJ. Extracellular vesicles in cancer - implications for future improvements in cancer care. *Nat Rev Clin Oncol.* 2018;15(10):617–638. doi:10.1038/s41571-018-0036-9
28. Zhou C, Zhang B, Yang Y, et al. Stem cell-derived exosomes: emerging therapeutic opportunities for wound healing. *Stem Cell Res Ther.* 2023;14(1):107. doi:10.1186/s13287-023-03345-0
29. Radosinska J, Bartekova M. Therapeutic Potential of Hematopoietic Stem Cell-Derived Exosomes in Cardiovascular Disease. *Adv Exp Med Biol.* 2017;998:221–235.
30. Mamidi N, De Silva FF, Vacas AB, et al. Multifaceted Hydrogel Scaffolds: bridging the Gap between Biomedical Needs and Environmental Sustainability. *Adv Healthc Mater.* 2024;13(27):e2401195. doi:10.1002/adhm.202401195
31. Jiang L, Vader P, Schiffelers RM. Extracellular vesicles for nucleic acid delivery: progress and prospects for safe RNA-based gene therapy. *Gene Ther.* 2017;24(3):157–166. doi:10.1038/gt.2017.8
32. Walker S, Busatto S, Pham A, et al. Extracellular vesicle-based drug delivery systems for cancer treatment. *Theranostics.* 2019;9(26):8001–8017. doi:10.7150/thno.37097
33. El Andaloussi S, Lakhal S, Mager I, Wood MJ. Exosomes for targeted siRNA delivery across biological barriers. *Adv Drug Deliv Rev.* 2013;65(3):391–397. doi:10.1016/j.addr.2012.08.008
34. Vader P, Mol EA, Pasterkamp G, Schiffelers RM. Extracellular vesicles for drug delivery. *Adv Drug Deliv Rev.* 2016;106(Pt A):148–156. doi:10.1016/j.addr.2016.02.006
35. Mamidi N, Garcia RG, Martinez JDH, et al. Recent Advances in Designing Fibrous Biomaterials for the Domain of Biomedical, Clinical, and Environmental Applications. *ACS Biomater Sci Eng.* 2022;8(9):3690–3716. doi:10.1021/acsbomaterials.2c00786
36. Zhao L, Gu C, Gan Y, Shao L, Chen H, Zhu H. Exosome-mediated siRNA delivery to suppress postoperative breast cancer metastasis. *J Control Rel.* 2020;318:1–15. doi:10.1016/j.jconrel.2019.12.005
37. Xu S, Liu B, Fan J, et al. Engineered mesenchymal stem cell-derived exosomes with high CXCR4 levels for targeted siRNA gene therapy against cancer. *Nanoscale.* 2022;14(11):4098–4113. doi:10.1039/D1NR08170E
38. Yin T, Wang N, Jia F, et al. Exosome-based WTAP siRNA delivery ameliorates myocardial ischemia-reperfusion injury. *Eur J Pharm Biopharm.* 2024;197:114218. doi:10.1016/j.ejpb.2024.114218
39. Zhang H, Yan W, Wang J, et al. Surface functionalization of exosomes for chondrocyte-targeted siRNA delivery and cartilage regeneration. *J Control Rel.* 2024;369:493–505. doi:10.1016/j.jconrel.2024.04.009
40. Lai CP, Mardini O, Ericsson M, et al. Dynamic biodistribution of extracellular vesicles in vivo using a multimodal imaging reporter. *ACS Nano.* 2014;8(1):483–494. doi:10.1021/nn404945r
41. Wiklander OP, Nordin JZ, O'Loughlin A, et al. Extracellular vesicle in vivo biodistribution is determined by cell source, route of administration and targeting. *J Extracell Vesicles.* 2015;4(1):26316. doi:10.3402/jev.v4.26316
42. Zipkin M. Big pharma buys into exosomes for drug delivery. *Nature Biotechnol.* 2020;38(11):1226–1228. doi:10.1038/s41587-020-0725-7
43. Pan S, Zhang Y, Natalia A, et al. Extracellular vesicle drug occupancy enables real-time monitoring of targeted cancer therapy. *Nat Nanotechnol.* 2021;16(6):734–742. doi:10.1038/s41565-021-00872-w
44. Zhang K, Li R, Chen X, et al. Renal Endothelial Cell-Targeted Extracellular Vesicles Protect the Kidney from Ischemic Injury. *Adv Sci.* 2023;10(3):e2204626. doi:10.1002/advs.202204626
45. Alvarez-Erviti L, Seow Y, Yin H, Betts C, Lakhal S, Wood MJ. Delivery of siRNA to the mouse brain by systemic injection of targeted exosomes. *Nature Biotechnol.* 2011;29(4):341–345. doi:10.1038/nbt.1807
46. Liu Q, Li D, Pan X, Liang Y. Targeted therapy using engineered extracellular vesicles: principles and strategies for membrane modification. *J Nanobiotechnol.* 2023;21(1):334. doi:10.1186/s12951-023-02081-0
47. Armstrong JP, Holme MN, Stevens MM. Re-Engineering Extracellular Vesicles as Smart Nanoscale Therapeutics. *ACS Nano.* 2017;11(1):69–83. doi:10.1021/acsnano.6b07607

48. Hosseini NF, Amini R, Ramezani M, Saidijam M, Hashemi SM, Najafi R. AS1411 aptamer-functionalized exosomes in the targeted delivery of doxorubicin in fighting colorectal cancer. *Biomed Pharmacother.* **2022**;155:113690. doi:10.1016/j.biopha.2022.113690
49. Zheng D, Ruan H, Chen W, et al. Advances in extracellular vesicle functionalization strategies for tissue regeneration. *Bioact Mater.* **2023**;25:500–526. doi:10.1016/j.bioactmat.2022.07.022
50. Luo ZW, Li FX, Liu YW, et al. Aptamer-functionalized exosomes from bone marrow stromal cells target bone to promote bone regeneration. *Nanoscale.* **2019**;11(43):20884–20892. doi:10.1039/C9NR02791B
51. Han Q, Xie QR, Li F, et al. Targeted inhibition of SIRT6 via engineered exosomes impairs tumorigenesis and metastasis in prostate cancer. *Theranostics.* **2021**;11(13):6526–6541. doi:10.7150/thno.53886
52. Hosseini Shamili F, Alibolandi M, Rafatpanah H, et al. Immunomodulatory properties of MSC-derived exosomes armed with high affinity aptamer toward myelin as a platform for reducing multiple sclerosis clinical score. *J Control Rel.* **2019**;299:149–164. doi:10.1016/j.jconrel.2019.02.032
53. Ma W, Yang Y, Zhu J, et al. Biomimetic Nanoerythrocyte-Coated Aptamer–DNA Tetrahedron/Maytansine Conjugates: pH-Responsive and Targeted Cytotoxicity for HER2-Positive Breast Cancer. *Adv Mater.* **2022**;34(46):e2109609. doi:10.1002/adma.202109609
54. Wu T, Liu Y, Cao Y, Liu Z. Engineering Macrophage Exosome Disguised Biodegradable Nanoplatform for Enhanced Sonodynamic Therapy of Glioblastoma. *Adv Mater.* **2022**;34(15):e2110364. doi:10.1002/adma.202110364
55. Aghajanian H, Kimura T, Rurik JG, et al. Targeting cardiac fibrosis with engineered T cells. *Nature.* **2019**;573:7774:430–433. doi:10.1038/s41586-019-1546-z
56. Sun Y, Ma M, Cao D, et al. Inhibition of Fap Promotes Cardiac Repair by Stabilizing BNP. *Circulation Research.* **2023**;132(5):586–600. doi:10.1161/CIRCRESAHA.122.320781
57. Livak KJ, Schmittgen TD. Analysis of relative gene expression data using real-time quantitative PCR and the 2⁻(Delta Delta C(T)) Method. *Methods.* **2001**;25(4):402–408. doi:10.1006/meth.2001.1262
58. Bujak M, Frangogiannis NG. The role of TGF-beta signaling in myocardial infarction and cardiac remodeling. *Cardiovas Res.* **2007**;74(2):184–195. doi:10.1016/j.cardiores.2006.10.002
59. Xia Y, Lee K, Li N, Corbett D, Mendoza L, Frangogiannis NG. Characterization of the inflammatory and fibrotic response in a mouse model of cardiac pressure overload. *Histochem Cell Biol.* **2009**;131(4):471–481. doi:10.1007/s00418-008-0541-5
60. Dobaczewski M, Chen W, Frangogiannis NG. Transforming growth factor (TGF)-beta signaling in cardiac remodeling. *J mol Cell Cardiol.* **2011**;51(4):600–606. doi:10.1016/j.yjmcc.2010.10.033
61. Schultz Jel J, Witt SA, Glascock BJ, et al. TGF-beta1 mediates the hypertrophic cardiomyocyte growth induced by angiotensin II. *J Clin Invest.* **2002**;109(6):787–796. doi:10.1172/JCI0214190
62. Bujak M, Ren G, Kweon HJ, et al. Essential role of Smad3 in infarct healing and in the pathogenesis of cardiac remodeling. *Circulation.* **2007**;116(19):2127–2138. doi:10.1161/CIRCULATIONAHA.107.704197
63. Yuan SM, Jing H. Cardiac pathologies in relation to Smad-dependent pathways. *Interact Cardiovasc Thorac Surg.* **2010**;11(4):455–460. doi:10.1510/ivts.2010.234773
64. Meng Z, Li HY, Si CY, Liu YZ, Teng S. Asiatic acid inhibits cardiac fibrosis through Nrf2/HO-1 and TGF-beta1/Smads signaling pathways in spontaneous hypertension rats. *Int Immunopharmacol.* **2019**;74:105712. doi:10.1016/j.intimp.2019.105712
65. Kang JY, Kim H, Mun D, Yun N, Joung B. Co-delivery of curcumin and miRNA-144-3p using heart-targeted extracellular vesicles enhances the therapeutic efficacy for myocardial infarction. *J Control Rel.* **2021**;331:62–73. doi:10.1016/j.jconrel.2021.01.018
66. Xu R, Greening DW, Zhu HJ, Takahashi N, Simpson RJ. Extracellular vesicle isolation and characterization: toward clinical application. *J Clin Invest.* **2016**;126(4):1152–1162. doi:10.1172/JCI81129
67. Usman WM, Pham TC, Kwok YY, et al. Efficient RNA drug delivery using red blood cell extracellular vesicles. *Nat Commun.* **2018**;9(1):2359. doi:10.1038/s41467-018-04791-8
68. Batrakova EV, Kim MS. Using exosomes, naturally-equipped nanocarriers, for drug delivery. *J Control Rel.* **2015**;219:396–405. doi:10.1016/j.jconrel.2015.07.030
69. Jang HJ, Shim KS, Lee J, et al. Engineering of Cell Derived-Nanovesicle as an Alternative to Exosome Therapy. *Tissue Eng Regen Med.* **2024**;21(1):1–19. doi:10.1007/s13770-023-00610-4
70. Jo W, Kim J, Yoon J, et al. Large-scale generation of cell-derived nanovesicles. *Nanoscale.* **2014**;6(20):12056–12064. doi:10.1039/C4NR02391A
71. Chen C, Wang J, Sun M, Li J, Wang HD. Toward the next-generation phyto-nanomedicines: cell-derived nanovesicles (CDNs) for natural product delivery. *Biomed Pharmacother.* **2022**;145:112416. doi:10.1016/j.biopha.2021.112416
72. Balaj L, Lessard R, Dai L, et al. Tumour microvesicles contain retrotransposon elements and amplified oncogene sequences. *Nat Commun.* **2011**;2(1):180. doi:10.1038/ncomms1180
73. Kang JY, Park H, Kim H, et al. Human peripheral blood-derived exosomes for microRNA delivery. *Int J Mol Med.* **2019**;43(6):2319–2328. doi:10.3892/ijmm.2019.4150
74. Zhang J, Ji C, Zhang H, et al. Engineered neutrophil-derived exosome-like vesicles for targeted cancer therapy. *Sci Adv.* **2022**;8(2):eabj8207. doi:10.1126/sciadv.abj8207
75. Zheng G, Ma HW, Xiang GH, et al. Bone-targeting delivery of platelet lysate exosomes ameliorates glucocorticoid-induced osteoporosis by enhancing bone-vessel coupling. *J Nanobiotechnol.* **2022**;20(1):220. doi:10.1186/s12951-022-01400-1
76. Yuan Z, Hu H, Zhu Y, et al. Colorectal cancer cell intrinsic fibroblast activation protein alpha binds to Enolase1 and activates NF-kappaB pathway to promote metastasis. *Cell Death Dis.* **2021**;12(6):543. doi:10.1038/s41419-021-03823-4
77. Fitzgerald AA, Weiner LM. The role of fibroblast activation protein in health and malignancy. *Cancer Metastasis Rev.* **2020**;39(3):783–8030. doi:10.1007/s10555-020-09909-3
78. Hallal S, Tuzesi A, Grau GE, Buckland ME, Alexander KL. Understanding the extracellular vesicle surface for clinical molecular biology. *J Extracell Vesicles.* **2022**;11(10):e12260. doi:10.1002/jev2.12260

International Journal of Nanomedicine**Publish your work in this journal**

The International Journal of Nanomedicine is an international, peer-reviewed journal focusing on the application of nanotechnology in diagnostics, therapeutics, and drug delivery systems throughout the biomedical field. This journal is indexed on PubMed Central, MedLine, CAS, SciSearch®, Current Contents®/Clinical Medicine, Journal Citation Reports/Science Edition, EMBase, Scopus and the Elsevier Bibliographic databases. The manuscript management system is completely online and includes a very quick and fair peer-review system, which is all easy to use. Visit <http://www.dovepress.com/testimonials.php> to read real quotes from published authors.

Submit your manuscript here: <https://www.dovepress.com/international-journal-of-nanomedicine-journal>

Dovepress
Taylor & Francis Group